Complete phase behavior of the symmetrical colloidal electrolyte

José B. Caballero[a)]
Department of Applied Physics, University of Almeria, E-04120 Almeria, Spain

Eva G. Noya and Carlos Vega
Departamento de Química-Física, Facultad de Ciencias Químicas, Universidad Complutense de Madrid, E-28040 Madrid, Spain

(Received 2 July 2007; accepted 31 October 2007; published online 28 December 2007)

We computed the complete phase diagram of the symmetrical colloidal electrolyte by means of Monte Carlo simulations. Thermodynamic integration, together with the Einstein-crystal method, and Gibbs-Duhem integration were used to calculate the equilibrium phase behavior. The system was modeled via the linear screening theory, where the electrostatic interactions are screened by the presence of salt in the medium, characterized by the inverse Debye length, κ (in this work $\kappa\sigma=6$). Our results show that at high temperature, the hard-sphere picture is recovered, i.e., the liquid crystallizes into a fcc crystal that does not exhibit charge ordering. In the low temperature region, the liquid freezes into a CsCl structure because charge correlations enhance the pairing between oppositely charged colloids, making the liquid-gas transition metastable with respect to crystallization. Upon increasing density, the CsCl solid transforms into a CuAu-like crystal and this one, in turn, transforms into a tetragonal ordered crystal near close packing. Finally, we have studied the ordered-disordered transitions finding three triple points where the phases in coexistence are liquid–CsCl–disordered fcc, CsCl–CuAu–disordered fcc, and CuAu–tetragonal–disordered fcc.
© *2007 American Institute of Physics*. [DOI: 10.1063/1.2816707]

I. INTRODUCTION

Colloids are important in different fields, such as in nanotechnology, biology, and physics. The main advantage of such systems is the facility to manipulate the shape and the physics governing their properties. One potential application of colloids is the creation of photonic crystals. In this field, colloidal electrolytes (a mixture of oppositely spherical charged colloids) have recently been studied experimentally, and different superlattice crystals were reported, some of them without an atomic counterpart.[1,2] These colloidal mixtures can be considered as the colloidal analog to the widely studied ionic fluids, physically modeled by primitive models, where the particles are represented by hard spheres with punctual charges located at the center of the spheres. The most important ionic system is the symmetrical one [represented by the restricted primitive model (RPM)] because it represents the most simple charged system showing effects due to strong electrostatic coupling phenomena.[3]

The phase behavior of the RPM has been extensively studied by means of computer simulations.[4–10] In the same way, computer simulations have been used to calculate the phase diagram of colloidal electrolytes[10–13] (also recently extended to nonequilibrium situations[14]). In these studies, two different models have been used, both consisting of an effective interaction that considers repulsions at short distances and long-ranged electrostatic interactions modeled via the lineal electrostatic screening theory, mediated by the presence of salt in the medium. One of us used an exponential law to describe the electrostatic interaction,[12–15] while Hynninen and co-workers employed a Yukawa potential.[10,11] The gas-liquid transition has been studied for these two models and, indeed, both produce similar results.[11–13] However, the equilibrium crystal phases have been studied only for the Yukawa model,[10] showing an exciting phase diagram. As expected, the complete phase behavior is qualitatively similar to that one of the RPM.[7,10] Concretely, at high temperatures, the hard-sphere limit is recovered, as the electrostatic interactions are negligible. Thus, the liquid freezes into a disordered fcc crystal (cubic symmetry) upon compression, being this transition first order. At lower temperatures, three different crystalline phases exist (see Fig. 1): CsCl (cubic symmetry), CuAu-like crystal (tetragonal symmetry), and a tetragonal ordered solid which was first observed for the RPM model[7] and, therefore, we will call it RPM crystal. Observe that the CsCl and CuAu-like crystals have the same base, a positive particle at the origin and another at the center of the parallelepiped that forms the unit cell. However, whereas the CsCl crystal has cubic symmetry, the CuAu structure is tetragonal. Interestingly, the CuAu structure can be transformed into the CsCl crystal simply by shortening the c edge of the CuAu structure up to $c/a=1/\sqrt{2}$ [see Fig. 1(C)]. Inversely, the CuAu crystal can be obtained by increasing the c edge of this structure up to $c/a=\sqrt{2}$ [see Fig. 1(B)]. Finally, it is worth observing that in the RPM crystal [Fig. 1(D)], the particles are located at fcc positions but, due to the presence of two types of particles, this structure does not have a cubic symmetry.

So far the complete phase diagram is lacking for the exponential model. Thus, the main aim of this work will be its calculation. On one hand, our work will serve to check

a)Electronic mail: jcaballe@ual.es.

 © 2007 American Institute of Physics

Downloaded 08 Jan 2008 to 147.96.6.138. Redistribution subject to AIP license or copyright; see http://jcp.aip.org/jcp/copyright.jsp

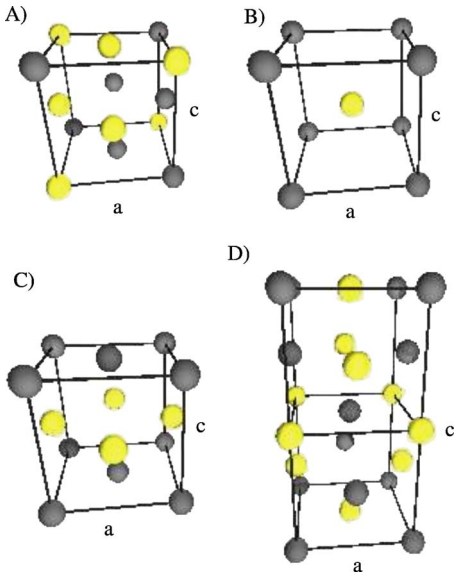

FIG. 1. (Color online) Different crystal phases present in colloidal electrolytes: (A) disordered fcc (cubic symmetry), (B) CsCl (cubic symmetry), (C) CuAu (tetragonal symmetry), and (D) RPM crystal (tetragonal symmetry). Note that structure (C) is a tetragonal CsCl crystal with $c/a=\sqrt{2}$. Analogously, a CsCl crystal can be considered as a tetragonal CuAu-like structure with $c/a=1/\sqrt{2}$.

that the physics for colloidal electrolytes is similar using either the Yukawa model or the exponential model. Moreover, we will study the solid-solid phase transitions in detail. The paper is organized as follows: Sections II and III are devoted to describe the model potential and the simulation details. Then, the way in which the phase diagram has been calculated is detailed in Sec. IV. Finally, Sec. V remarks the main conclusions of this work.

II. MODEL

We consider the symmetrical colloidal electrolyte as a mixture of N spherical colloidal particles with diameter σ, $N/2$ carrying a surface potential $+\epsilon$ and the other $N/2$ with surface potential $-\epsilon$. The mixture is immersed in a continuous medium characterized by a dielectric constant in presence of an electrolyte. The interactions between the colloidal particles were modeled by the following potential function:[16]

$$U(r)=\begin{cases}\infty, & r\leqslant\sigma\\ \pm\varepsilon\exp\{-\kappa(r-\sigma)\}, & r>\sigma,\end{cases} \quad (1)$$

where ε is in the appropriate units and κ is the inverse Debye length, which depends on the salt concentration: Increasing κ means to shorten the interaction range. For computational reasons, the potential was truncated at the distance at which $U(r_{\text{cut}})/\varepsilon=5\times10^{-4}$, which for $\kappa\sigma=6$ corresponds to a distance $r_{\text{cut}}/\sigma=2.3$. Note that the only difference between this model and the one used in Refs. 10 and 11 is a factor σ/r $[U_{\text{Yukawa}}(r)=\pm\epsilon\sigma e^{-\kappa(r-\sigma)}/r]$. Both models present the same limit at high $\kappa\sigma$. However, at low $\kappa\sigma$ values, the models represent different physical pictures. In particular, the Yukawa model tends to the RPM model, while the exponential model exhibits a different limit behavior. However, this work is concerned just with a relatively large value of $\kappa\sigma$, i.e., $\kappa\sigma=6$ and, for this value, both models predict similar results (compare the gas-liquid binodals in Refs. 11 and 12). Another comparison between both models can be made by computing Boyle temperature, which is related to the pair interactions between particles. We have found that the exponential model with $\kappa\sigma=6$ can be mapped into the Yukawa model with $\kappa\sigma=5$, as both show an approximately equal Boyle temperature ($k_BT_{\text{Boyle}}/\varepsilon\approx0.43$). In fact, in general, we have found that the exponential model with $\kappa\sigma$ has a similar Boyle temperature to that of the Yukawa model with $(\kappa-1)\sigma$. We checked that this mapping was working quite well from $\kappa\sigma=4$ to 20. However, for values of $\kappa\sigma$ smaller than 4, the differences between both models become significant.

It is important to remember that Eq. (1) is just an approximation to the whole problem, where the small ions are not explicitly simulated but they are implicitly included in the potential. It is very likely that the phase diagram will be changed by the inclusion of the microions. In particular, two coexisting phases will normally have different concentrations of small ions, and this is not taken into account by Eq. (1) (note that the same value of the $\kappa\sigma$ is being used for all phases appearing in the phase diagram). As a consequence, it is very likely that the phase diagram will be changed if the microions are explicitly included, especially the coexistence lines between two phases with very different densities.[17] At present, a rigorous computation of the phase diagram including all the particles seems extremely difficult[18] and, for this reason, it seems reasonable to study first the behavior of a simple model before introducing the microions rigorously.

Throughout, standard reduced units will be used: $\sigma=1$ being the diameter of the particles and ε the energy scale. Hence, the reduced temperature will be $T^*=k_BT/\varepsilon$ (superscript asterisks mark reduced units), the reduced density $\rho^*=N\sigma^3/V$, and the reduced pressure $P^*=P\sigma^3/\varepsilon$. Using reduced units, the only parameter that needs to be specified to fully characterize the interaction between the particles is the inverse Debye lenght κ, which in this work was set to $\kappa\sigma=6$. This selection was motivated because previous calculations using the Yukawa model showed that the gas-liquid transition becomes metastable with respect to solidification from beyond around $\kappa\sigma=4.5-6$.[11] Moreover, the complete phase diagram of the Yukawa model has been computed for this same value $\kappa\sigma=6$. Therefore, our results would serve to see if the gas-liquid transition becomes metastable at this value of κ and to study the possible effect of the potential model (exponential or Yukawa) in the phase behavior.

III. SIMULATION DETAILS

Coexistence points can be estimated with the thermodynamics integration methodology.[19] The method consists in estimating the free energy of the phases and then the coexistence points are obtained by imposing thermodynamic equilibrium conditions: Equal temperature, pressure, and chemical potential. Determining absolute free energies from computer simulations is a tough task, but it is easy to compute derivatives of it, as the pressure

Downloaded 08 Jan 2008 to 147.96.6.138. Redistribution subject to AIP license or copyright; see http://jcp.aip.org/jcp/copyright.jsp

$$P = -\left(\frac{\partial F}{\partial V}\right)_{N,T}, \tag{2}$$

being F the Helmholtz free energy and V the volume. By integrating this equation, estimations of free energy differences can be readily obtained. However, to obtain the value of the absolute free energy, it is necessary to know the free energy of a reference state. For the fluid phase, the ideal gas is a natural election as reference system and using Eq. (2), then

$$\frac{F(\rho)}{Nk_BT} = \frac{F_{\mathrm{id}}(\rho)}{Nk_BT} + \frac{1}{k_BT}\int_0^{\rho} d\rho' \frac{P(\rho') - \rho' k_BT}{\rho'^2}, \tag{3}$$

where $F_{\mathrm{id}}(\rho)$ is the free energy of an ideal gas at density ρ. The free energy of the fluid phase can be estimated by integration of the equation of state from the very low density limit, which can be obtained from Monte Carlo (MC) simulations. An important condition for this method to be valid is that the path along which the integral is performed must be reversible, i.e., first-order phase transitions must be avoided. In the same way, the free energy of a solid phase can be estimated as

$$\frac{F(\rho)}{Nk_BT} = \frac{F_0(\rho_0)}{Nk_BT} + \frac{1}{k_BT}\int_{\rho_0}^{\rho} d\rho' \frac{P(\rho')}{\rho'^2}, \tag{4}$$

where $F_0(\rho_0)$ is the free energy of the solid at the reference state ρ_0. That is, to use the thermodynamic integration in solid phases, the absolute free energy in a reference point must be known. The free energy of crystal phases can be obtained using the Einstein crystal technique, with the Frenkel-Ladd methodology.[20] In this method, the free energy of a given crystal is obtained by integration to an Einstein-crystal with fixed center of mass, whose free energy is already known. Using the Einstein-crystal method, the Helmholtz free energy can be computed as the sum of four terms,

$$F = F_E + \Delta F_1 + \Delta F_2 + \Delta F_3, \tag{5}$$

where F_E is the free energy of an ideal noninteracting Einstein crystal, ΔF_1 is free energy difference between the colloidal electrolyte solid and the Einstein crystal supplemented with our model potential [Eq. (1)], ΔF_2 denotes the free energy difference between the interacting and noninteracting Einstein crystals, and ΔF_3 is the free energy difference between a system with an unconstrained center of mass and the one with fixed center of mass. Expressions for these terms can be found in Refs. 19–21.

Once a coexistence point is well established, Gibbs-Duhem integration can be used to determine the complete coexistence line.[22] In this method, the Clapeyron equation is solved numerically,

$$\left(\frac{dP}{dT}\right)_{\mathrm{coex}} = \frac{\Delta h}{T\Delta v}, \tag{6}$$

being Δh and Δv the enthalpy and volume changes per particle, respectively, between the two coexisting phases. In order to solve Eq. (6), a fourth-order Runge-Kutta algorithm was implemented, and the slope was estimated performing *NPT* MC simulations of the two coexisting phases.

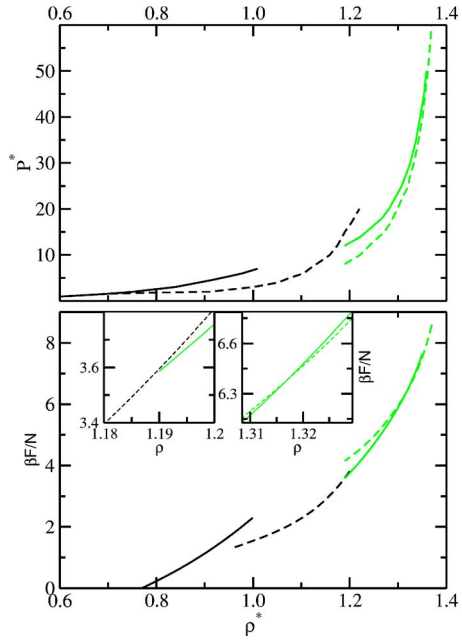

FIG. 2. (Color online) Upper panel: Equations of state of the colloidal electrolyte ($\kappa\sigma=6$) for different phases at $T^*=0.5$, liquid (solid line), CsCl (dashed line), CuAu (gray solid line, where c/a changes), and RPM crystal (gray dashed line). Lower panel: The same as above for the free energy. Insets are enlargements around CsCl–CuAu and CuAu-RPM crystal transitions.

In all the MC runs, the simulation box contained 250 particles for the CsCl crystal, whereas 256 particles were used for all the other phases (fluid, disordered fcc, CuAu-like, and tetragonal crystals). All the simulations were started with three-dimensional replications of the snapshots shown in Fig. 1. The simulations comprise typically 50 000 MC cycles for equilibration and 100 000 cycles for obtaining averages. When the CuAu-like phase was involved, we performed *NPT* MC simulations with anisotropic scaling (i.e., the lengths of the edges of the simulation box were allowed to change independently, thus allowing the c/a ratio to change).

IV. EQUILIBRIUM PHASE DIAGRAM

The equations of state were obtained by means of *NPT* MC simulations using isotropic scaling for the fluid phase and the CsCl, disordered fcc, and RPM crystals. Even though the RPM crystal has tetrahedral symmetry, we expect that the edges of the box would maintain the ratio $c'/a=1$ (where $c'=c/2$, see Fig. 1), in analogy to what happened for the RPM system.[9] Indeed, some preliminary *NPT* simulations with anisotropic scaling showed that the system relaxed to the ratio $c'/a=1$ and, therefore, we decided to use isotropic scaling in our *NPT* simulations. For the CuAu case, however, it was necessary to perform *NPT* simulations with anisotropic scaling, so that the equilibrium c/a ratio could be obtained. Figure 2 shows the equation of state for the liquid and crystal phases for the colloidal electrolyte represented by Eq. (1) with $\kappa\sigma=6$ at $T^*=0.5$ (note that this isotherm is above the critical temperature[12]). While the estimation of the free energy for the liquid is straightforward combining Eq. (3) and the equation of state, for the solid, the use of Eq. (4)

Downloaded 08 Jan 2008 to 147.96.6.138. Redistribution subject to AIP license or copyright; see http://jcp.aip.org/jcp/copyright.jsp

TABLE I. Tabulated data of the free energy at several state points using the Einstein-crystal method for different structures (c/a refers to labels in Fig. 1, $c'=c/2$ for the RPM crystal). For the CuAu structure, the ratio c/a was obtained from *NPT* runs with anisotropic scaling of the simulation box, except for the case marked with an asterisk in the table, where the value $c/a=1$ was imposed to show the large increase of free energy when the ratio c/a is not the one that corresponds to the relaxed structure.

ρ^*, T^*	Crystal	N	F/NK_BT
1.25, 0.17	CsCl ($c/a=1$)	250	−4.161
1.25, 0.3	CsCl ($c/a=1$)	250	2.036
1.14, 0.5	CsCl ($c/a=1$)	250	2.745
1.10, 1.0	CsCl ($c/a=1$)	250	4.193
1.25, 1.1	CsCl ($c/a=1$)	250	4.364
1.35, 0.17	CuAu ($c/a=0.965$)	256	0.603
1.212, 0.3	CuAu ($c/a=0.924$)	256	3.148
1.25, 0.5*	CuAu ($c/a=1$)	256	5.089
1.25, 0.5	CuAu ($c/a=0.90$)	256	4.698
1.25, 1.0	CuAu ($c/a=0.96$)	256	6.405
1.25, 1.1	CuAu ($c/a=0.97$)	256	6.540
1.35, 0.17	RPM ($c'/a=1$)	256	0.841
1.25, 0.3	RPM ($c'/a=1$)	256	2.985
1.25, 0.5	RPM ($c'/a=1$)	256	4.959
1.25, 1.0	RPM ($c'/a=1$)	256	6.437
1.25, 1.1	RPM ($c'/a=1$)	256	6.573

requires the knowledge of the free energy of the crystalline structure at one thermodynamic state. As it has been already mentioned, this was achieved using the Einstein-crystal method.[20] The free energies of all the crystal structures calculated with this technique are listed in Table I. Note that for the CsCl, disordered fcc, and RPM crystals, the parameter c/a was set to 1 (for the latter, $c'/a=1$, where $c'=c/2$). On the contrary, for CuAu-like crystals, this parameter is obtained from the anisotropic *NPT* simulations, where the ratio c/a is free to fluctuate. Also, it is interesting to observe that at $T^*=0.5$ and $\rho^*=1.25$, the tetragonal CuAu phase [see Fig. 1(C)] exhibits a higher free energy when $c/a=1$ than when $c/a\neq 1$, being even higher than that of the RPM crystal. This reflects the importance of using the proper relaxed value of c/a to compute the free energy. Once the free energy at a point is known, the free energy along the isotherm is easily drawn applying Eq. (4) (lower panel in Fig. 2).

A clear first-order phase transition occurs between the fluid and the CsCl solid. Since we have already determined the equation of state and the free energy of these phases, the coexistence densities can be estimated by imposing the equilibrium criteria (i.e., equal chemical potential, $\mu_1=\mu_2$, at a given pressure and temperature). Now, from this point, Gibbs-Duhem integration can be cast to calculate the liquid-CsCl transition line (the results are shown in Figs. 3 and 4 and partially tabulated in Table II.) Additionally, we know that the liquid transforms into two different crystalline structures depending on the temperature: at low temperatures, it freezes into a CsCl crystal, while at very high temperature, where the charge correlations are overcome by the entropy, the liquid freezes into a disordered fcc crystal,[10,15] such as in the hard-sphere model. Therefore, the liquid–disordered fcc coexistence line has been obtained using Gibbs-Duhem integration starting from the hard-sphere limit (whose coexistence point is more or less well established,[19,23,24] and we have taken the classical value given by Hoover and Ree[24]), including the possibility of charge exchanges in the solid phase. In addition to particle and volume moves, two oppositely charged colloids are randomly chosen and we attempt to swap their charges according to the canonical distribution function. The P^*-T^* and ρ^*-T^* coexistence lines are shown in Figs. 3 and 4 (also partially tabulated in Table II). Note that the crossing point between the liquid-CsCl and liquid–disordered fcc coexistence lines defines a triple point where the fluid, CsCl, and disordered fcc phases coexist. Moreover, in Fig. 4, we observe that the liquid-gas transition is metastable with respect to crystallization, as it was previously reported for the Yukawa model.[10]

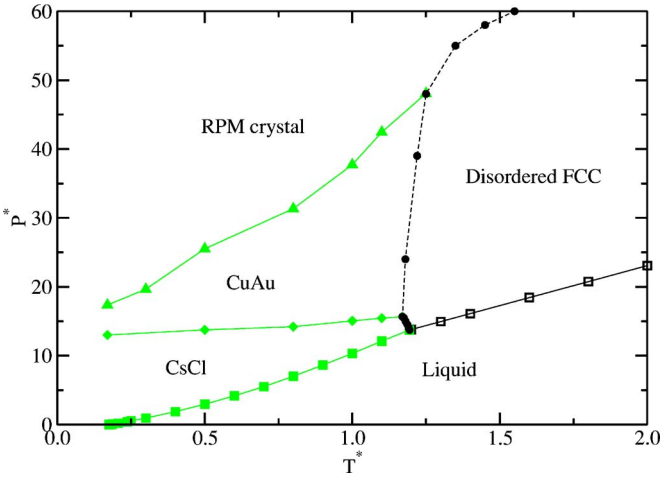

FIG. 3. (Color online) P^*-T^* phase diagram of the colloidal electrolyte with $\kappa\sigma=6$: Fluid–disordered fcc transition (open black squares), fluid-CsCl (filled gray squares), CsCl–CuAu (filled gray diamonds), CuAu–RPM crystal (filled gray triangles), and ordered-disordered transitions (filled black circles). Lines are only guides to the eye.

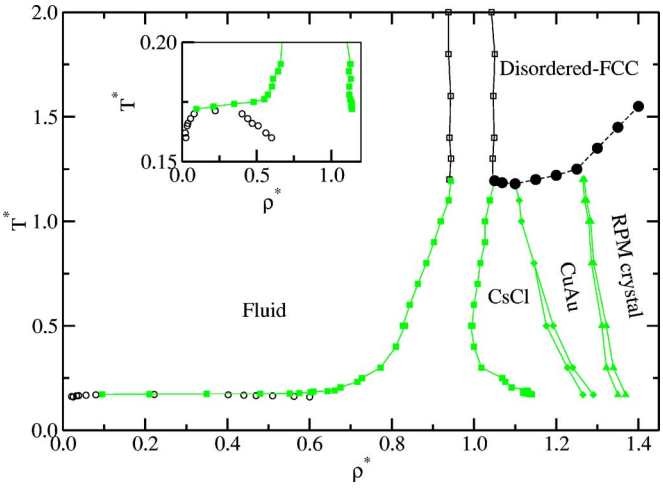

FIG. 4. (Color online) Equilibrium phase diagram of the colloidal electrolyte with $\kappa\sigma=6$: Gas-liquid from Gibbs ensemble Monte Carlo (open circles), liquid–disordered fcc from Gibbs-Duhem integration starting with the hard-sphere limit (open black squares), liquid-CsCl from Gibbs-Duhem starting with Einstein-crystal calculations (filled gray squares), CsCl–CuAu from free energy calculations (filled gray diamonds, Gibbs-Duhem integration produces the same results), CuAu–RPM crystal transition from free energy calculations (gray triangles), and ordered-disordered transitions (filled black circles). Lines are only guides to the eye. Inset: Enlargement around the critical region.

Downloaded 08 Jan 2008 to 147.96.6.138. Redistribution subject to AIP license or copyright; see http://jcp.aip.org/jcp/copyright.jsp

TABLE II. Coexistence conditions obtained with Gibbs-Duhem integration for different transitions.

T^*	P^*	ρ_1^*	ρ_2^*	u_1^*	u_2^*
		Liquid–disordered fcc			
100.0	1169	0.949	1.036	−0.007	−0.009
10.0	116.44	0.948	1.048	−0.15	−0.14
2.0	23.07	0.937	1.041	−0.52	−0.52
1.4	16.10	0.946	1.044	−0.65	−0.66
		Liquid–CsCl			
1.00	10.32	0.947	1.038	−0.85	−1.65
0.60	4.17	0.847	1.002	−0.99	−1.59
0.40	1.87	0.809	0.996	−1.13	−1.70
0.19	0.10	0.661	1.129	−1.29	−2.03
		CsCl–disordered fcc			
1.194	13.73	1.043	1.056	−1.60	−0.75
1.19	14.0	1.045	1.059	−1.62	−0.77
1.183	14.60	1.055	1.078	−1.69	−0.80

In Fig. 2, we also observe a weak CsCl–CuAu transition at $T^*=0.5$. This is a martensitic transition, which means that it is diffusionless, i.e., particle diffusion is not necessary to produce it. On the contrary, the transformation occurs by the deformation of the unit cell. In this case, the cubic unit cell (CsCl crystal) is transformed into a tetragonal unit cell (CuAu crystal). Figure 5 shows the equations of state for the CuAu-like crystal using anisotropic *NPT* simulations, where the evolution of the potential energy is also shown in one of the insets, as well as the equation of state of the CsCl crystal (in this case, using isotropic *NPT* simulations). Note that both equations of state coincide at low packing fractions, where the CuAu crystal presents a value $c/a \approx 1/\sqrt{2}$, which means that the crystal has transformed into the CsCl structure. On the contrary, at higher densities, the unit cell transforms into a tetragonal one where the relation is $1/\sqrt{2} \leqslant c/a \leqslant 1$. It is worth noting the energy evolution along this isotherm. In the CsCl region, the energy decreases continuously as the density increases, whereas the opposite behavior is found for the CuAu phase, what points out that this transition is driven by entropic effects. The CuAu exhibits a higher energy, but this structure can be packed more closely leading to a structure with higher density.

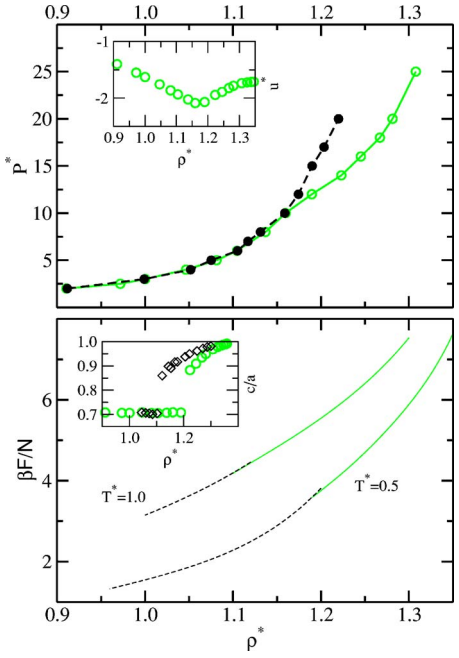

FIG. 5. (Color online) Upper panel: Equations of state for the colloidal electrolyte with $\kappa\sigma=6$ at $T^*=0.5$, black circles from isotropic *NPT* simulations for the CsCl crystal and gray circles from anisotropic simulations of the CuAu-like crystal (the inset shows the energy per particle evolution along this isotherm). Lower panel: Free energy of the CsCl (dashed lines) and CuAu-like crystals (solid lines) at two temperatures, $T^*=0.5$ and 1.0. Inset: The parameter c/a from anisotropic *NPT* simulations in the CuAu phase, $T^*=0.5$ (gray circles) and $T^*=1.0$ (black diamonds). Remember that when $c/a \approx 0.7$, the crystal recovers the cubic symmetry of the CsCl structure.

Once that we have determined an initial coexistence point, Eq. (6) can be used to determine the complete transition line. However, we found that the CuAu crystal tends to convert into the CsCl crystal because the coexistence densities for both phases are very similar and, hence, the solutions of the Clapeyron equation are not reliable. Therefore, free energy calculations and thermodynamic integration were employed to estimate the coexistence densities, plotted in Figs. 3 and 4. Moreover, in Fig. 5, we show the free energies of both phases at two temperatures. Observe that at high temperature, the transition is much weaker than at low temperatures, although it is still producing a discontinuous change in the parameter c/a (inset of Fig. 5).

In addition, at higher densities, the CuAu–RPM crystal phase transition is present (see Fig. 2). Observe that this transition shall be carried out via the diffusion of the colloidal particles (see Fig. 1). This makes it difficult to observe it in experiments because diffusion is highly impeded at so high packing fractions.[1,2] This is, as well, a weak first-order transition, and the coexistence densities are rather similar, which makes it difficult to study via Gibbs-Duhem integration. Therefore, the results shown in Figs. 3 and 4 for such a transition have been estimated from free energy estimations. It is interesting to observe that the most stable phase at $T^*=0$ and close packing is the RPM crystal, as its internal energy is lower ($U^*/N=-0.387$ for the RPM crystal and $U^*/N=-0.328$ for the CuAu crystal).

So far, we have studied the phases that are stable at low temperature for the colloidal electrolyte, as well as the way in which they transform into each other. As we know, at very high temperatures, the crystalline phase will be that one of the hard-sphere case, that is, a disordered fcc. Thus, three different ordered-disordered transitions will occur: CsCl–disordered fcc, CuAu–disordered fcc, and RPM crystal–disordered fcc. First of all, we would like to point out that the estimation of this transition is a difficult task because the Einstein-crystal methodology does not work efficiently for the disordered crystal. In this technique, the free energy of a solid phase is computed for one particular snapshot of the crystal. Therefore, the calculated free energy is not correct when there are many possible configurations, as is the case of this crystal, unless all these configurations have the same statistical weight as, for example, in ice.[25] However, this is not the case here and, hence, we did not estimate these transition lines from free energy calculations. Instead, to trace

Downloaded 08 Jan 2008 to 147.96.6.138. Redistribution subject to AIP license or copyright; see http://jcp.aip.org/jcp/copyright.jsp

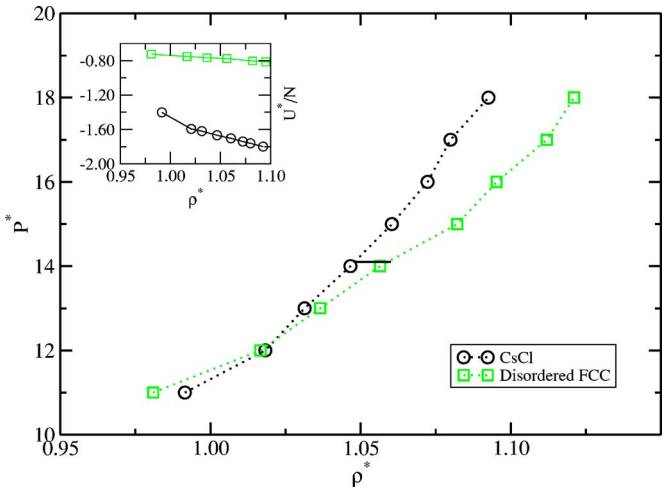

FIG. 6. (Color online) Equations of state at $T^*=1.19$ for the disordered fcc and the CsCl crystals around the region where the CsCl–disordered fcc transition takes places. Solid line indicates the coexistence pressure at this temperature. Inset: The same as in the main panel for the energy per particle.

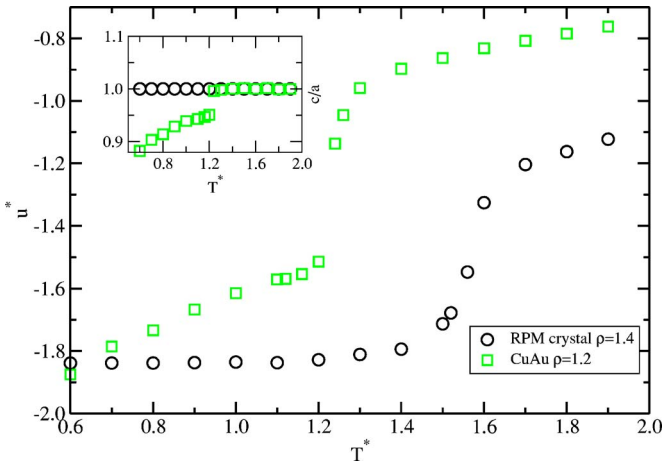

FIG. 7. (Color online) Ordered-disordered transitions from *NVT* simulations, where charge switch and shape moves were implemented, along two isochores: circles for RPM crystal at $\rho^*=1.4$ and squares for CuAu-like at $\rho^*=1.2$. Inset: The same as in the main panel for the parameter c/a (c'/a for the RPM structure).

the CsCl–disordered fcc coexistence line, Gibbs-Duhem integration was used starting from the triple point: Liquid–CsCl–disordered fcc. In this case, the densities of both phases were very similar, but both phases remained stable during the simulations. The results for this transition have been plotted in Figs. 3 and 4 (also tabulated in Table II). Interestingly, the slope in the P^*-T^* phase diagram is negative, what is an unusual behavior. To understand this slope, we have studied the equations of state of these phases at $T^*=1.19$ (Fig. 6), where the energy evolution along this isotherm is also shown. Looking at this plot (see also Table II), we can now rationalize this behavior inserting these values into the Clapeyron equation [Eq. (6)]: The enthalpy change will be positive, while the volume change will be negative. This means that the slope will be negative. Although this is an unusual behavior, it is not in contradiction with the Bridgman statements:[26] Upon heating at constant pressure, transitions are always endothermic, and increasing P^* at constant T^*, transitions always occur with a decrease of volume (this rule is of course compatible with positive and negative slopes).

Finally, we studied the CuAu–disordered fcc and RPM crystal–disordered fcc transitions. Gibbs-Duhem integration from the CsCl–CuAu–disordered fcc triple point could not be used to study the CuAu–disordered fcc transition because the systems were not stable; instead, they transform into each other. Therefore, we performed *NVT* simulations along isochores where we implement charge exchanges between two oppositely charged particles and attempt to change the relation c/a keeping the total volume constant. Figure 7 represents the temperature evolution of the energy and the ratio c/a for the CuAu and the RPM crystal. We observe that the transition occurs over a range of temperatures. To gain insights in this transition, we present in Fig. 8 the probability of the sample to have a given energy per particle. Note that at low and high temperature there is one single peak. On the contrary, two peaks are clearly observed at intermediate T^*, just at the transition. On one hand, we now understand why Gibbs-Duhem integration is difficult to implement for studying such a transition. On the other hand, we also note the difficulty to locate the transition. Nevertheless, we estimate the transition temperature as the intermediate temperature between the lowest and highest temperatures that exhibit two peaks of the energy histogram. Results for these transitions are shown in Figs. 3 and 4.

Finally, it is worth observing that the addition of this line introduces two new triple points. In one of them, the fcc disordered, tetragonal, and CuAu crystals coexist in equilibrium, and another one where the coexistence is produced

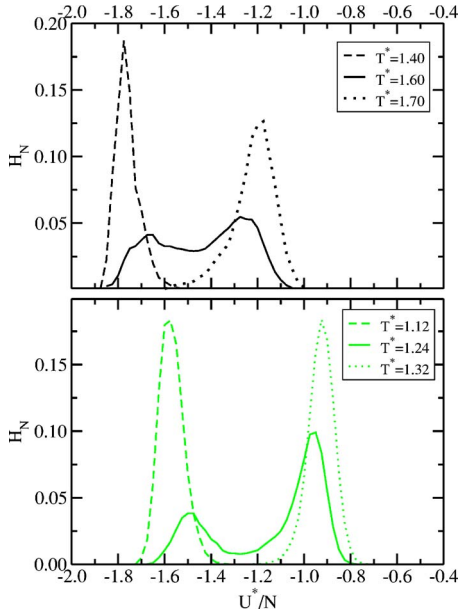

FIG. 8. (Color online) Probability of the system to have an energy per particle U^*/N for the isochores analyzed in Fig. 7. Upper panel: Temperature evolution of the energy probability at $\rho^*=1.40$, i.e., RPM crystal–disordered fcc transition. Lower panel: The same as before for the CuAu–disordered fcc transition at $\rho^*=1.20$. This plot shows the difficulty to mark the right place where this transition occurs, also pointing out the weakly first-order character of such a transition.

Downloaded 08 Jan 2008 to 147.96.6.138. Redistribution subject to AIP license or copyright; see http://jcp.aip.org/jcp/copyright.jsp

TABLE III. Thermodynamic states for the triple points in the symmetrical colloidal electrolyte with $\kappa\sigma=6$ (see Figs. 3 and 4).

Phases	P_t^*	T_t^*
Liquid–CsCl–dis. fcc	13.73	1.194
CsCl–CuAu–dis. fcc	15.66	1.180
CuAu–RPM crystal–dis. fcc	48.06	1.250

between CuAu, CsCl and fcc disordered. Table III lists the thermodynamic states of the triple points of the colloidal electrolyte modeled by Eq. (1) with $\kappa\sigma=6$.

V. CONCLUSIONS

We have studied the complete phase diagram of the symmetrical colloidal electrolyte with $\kappa\sigma=6$ modeled by the lineal screening theory via Eq. (1). In agreement with previous works[10] where the system was modeled with a slightly different interaction potential, several solid phases have been found. In addition to the fluid phase, which is stable at low packing fractions, CsCl, CuAu-like, and tetragonal ordered phases were found on increasing the density at low temperatures. All the transitions were identified to be first order, though at high temperatures the CsCl–CuAu transition is so weak that the simulations cannot display the difference in the coexistence densities. Interestingly, the liquid-gas transition is metastable with respect to crystallization.

At very high temperatures, the hard-sphere limit is recovered and the liquid is transformed by a first-order transition into a disordered fcc crystal. Thereby, three different ordered-disordered transitions exist: CsCl–disordered fcc, CuAu–disordered fcc, and RPM crystal–disordered fcc.

ACKNOWLEDGMENTS

The authors are grateful to A. M. Puertas for useful discussions. J.B.C. acknowledges the hospitality during his stay in the Universidad Complutense de Madrid, where part of these results were obtained. This work was supported by the Ministerio de Educación y Ciencia under Project Nos. MAT2004-03581 and FIS2007-66079-C02-01. E.G.N. wishes to thank the Ministerio de Educación y Ciencia and the Universidad Complutense de Madrid for a Juan de la Cierva fellowship.

[1] M. E. Leunissen, C. G. Christova, A. P. Hynninen, C. P. Royall, A. I. Campbell, A. Imhof, M. Dijkstra, R. van Roij, and A. van Blaaderen, Nature (London) **437**, 235 (2005).
[2] P. Bartlett and A. I. Campbell, Phys. Rev. Lett. **95**, 128302 (2005).
[3] M. E. Fisher and Y. Levin, Phys. Rev. Lett. **71**, 3826 (1993).
[4] B. Smit and D. Frenkel, Mol. Phys. **87**, 159 (1996).
[5] A. Z. Panagiotopoulous, J. Phys.: Condens. Matter **17**, S3205 (2005).
[6] C. Vega, F. Bresme, and J. L. F. Abascal, Phys. Rev. E **54**, 2746 (1996).
[7] F. Bresme, C. Vega, and J. L. F. Abascal, Phys. Rev. Lett. **85**, 3217 (2000).
[8] C. Vega, J. L. F. Abascal, C. McBride, and F. Bresme, J. Chem. Phys. **119**, 964 (2003).
[9] J. L. F. Abascal, C. Vega, C. McBride, and F. Bresme, Phys. Rev. E **68**, 052501 (2003).
[10] A. P. Hynninen, M. E. Leunissen, A. van Blaaderen, and M. Dijkstra, Phys. Rev. Lett. **96**, 018303 (2006).
[11] A. Fortini, A. P. Hynninen, and M. Dijkstra, J. Chem. Phys. **125**, 094502 (2006).
[12] J. B. Caballero, A. M. Puertas, A. Fernandez-Barbero, and F. J. De las Nieves, J. Chem. Phys. **121**, 2428 (2004).
[13] J. B. Caballero, A. M. Puertas, A. Fernandez-Barbero, F. J. De las Nieves, J. M. Enrique-Romero, and L. F. Rull, J. Chem. Phys. **124**, 054909 (2006).
[14] J. B. Caballero and A. M. Puertas, Phys. Rev. E **76**, 011401 (2007).
[15] J. B. Caballero and A. M. Puertas, THEOCHEM **769**, 157 (2006).
[16] B. V. Derjaguin and L. Landau, URSS **14**, 633 (1941); E. J. W. Verwey and J. T. G. Overweek, *Theory of the Stability of Lyophobic Colloids* (Elsevier, Amsterdam, 1948).
[17] M. S. Romero-Cano, J. B. Caballero, and A. M. Puertas, J. Phys. Chem. B **110**, 13220 (2006).
[18] R. Rydens, M. Ullner, and P. Linse, J. Chem. Phys. **123**, 034909 (2005).
[19] B. Smit and D. Frenkel, *Understanding Molecular Simulation* (Academic, New York, 1996).
[20] D. Frenkel and A. J. C. Ladd, J. Chem. Phys. **81**, 3188 (1984).
[21] C. Vega, E. A. P. Paras, and P. A. Monson, J. Chem. Phys. **96**, 9060 (1992).
[22] D. A. Kofke, Mol. Phys. **78**, 1331 (1993).
[23] J. M. Polson, E. Trizac, S. Pronk, and D. Frenkel, J. Chem. Phys. **112**, 5339 (2000).
[24] W. G. Hoover and F. H. Ree, J. Chem. Phys. **49**, 3609 (1971).
[25] E. Sanz, C. Vega, J. L. F. Abascal, and L. G. MacDowell, Phys. Rev. Lett. **92**, 255701 (2004).
[26] P. W. Bridgman, Proc. Am. Acad. Arts Sci. **47**, 441 (1912).

Downloaded 08 Jan 2008 to 147.96.6.138. Redistribution subject to AIP license or copyright; see http://jcp.aip.org/jcp/copyright.jsp